

## Anisotropic optical conductivity accompanied by a small energy gap in the one-dimensional thermoelectric telluride $\text{Ta}_4\text{SiTe}_4$

Fumiya Matsunaga,<sup>1</sup> Yoshihiko Okamoto<sup>1,2,\*</sup>, Yasunori Yokoyama<sup>1</sup>, Kanji Takehana,<sup>3</sup> Yasutaka Imanaka<sup>3</sup>,  
Yuto Nakamura,<sup>1</sup> Hideo Kishida<sup>1</sup>, Shoya Kawano,<sup>4</sup> Kazuyuki Matsuhira<sup>4</sup>, and Koshi Takenaka<sup>1</sup>

<sup>1</sup>Department of Applied Physics, Nagoya University, Furo-cho, Chikusa-ku, Nagoya 464–8603, Japan

<sup>2</sup>Institute for Solid State Physics, University of Tokyo, Kashiwanoha 5-1-5, Kashiwa 277–8581, Japan

<sup>3</sup>National Institute for Materials Science (NIMS), Sakura 3–13, Tsukuba 305–0003, Japan

<sup>4</sup>Graduate School of Engineering, Kyushu Institute of Technology, Kitakyushu 804–8550, Japan



(Received 8 September 2023; revised 31 January 2024; accepted 19 March 2024; published 8 April 2024)

We investigated the optical properties of single crystals of one-dimensional van der Waals crystal  $\text{Ta}_4\text{SiTe}_4$ , which exhibited high thermoelectric performance below room temperature. Optical conductivity estimated from reflectivity spectra indicates the presence of a small energy gap of 0.1–0.15 eV at the Fermi energy. At the lowest energy, optical conductivity along the  $\text{Ta}_4\text{SiTe}_4$  chain is an order of magnitude higher than that perpendicular to this direction, reflecting anisotropic electron conduction in  $\text{Ta}_4\text{SiTe}_4$ . These results suggest that the coexistence of a small band gap and moderate anisotropy in electron conduction is a promising strategy for developing high-performance thermoelectric materials for low-temperature applications.

DOI: [10.1103/PhysRevB.109.L161105](https://doi.org/10.1103/PhysRevB.109.L161105)

There are great expectations for thermoelectric energy conversion between thermal and electrical energies, which can be used for energy harvesting and local cooling. Currently, thermoelectric energy conversion has been practically used in Peltier cooling at around room temperature using  $\text{Bi}_2\text{Te}_3$ -based materials, and in radioisotope thermoelectric generators using PbTe- or SiGe-based materials. A new material that exhibits much higher performance at room temperature would open an avenue for the utility of energy harvesting, which obtains electrical energy from the surrounding temperature differences. In addition, a new material that exhibits high performance below  $-100$  °C, where  $\text{Bi}_2\text{Te}_3$ -based materials cannot be used, would lead to Peltier cooling and precision temperature control at low temperatures. Recently, the development of new materials for high-temperature applications has been remarkable. PbTe with hierarchical architectures,  $\text{AgPb}_m\text{SbTe}_{2+m}$ , and SnSe have been reported to exhibit considerably low thermal conductivity  $\kappa$ , resulting in a large dimensionless figure of merit  $ZT = S^2T/\rho\kappa$  exceeding 2 at high temperatures, where  $S$ ,  $\rho$ , and  $T$  are Seebeck coefficient, electrical resistivity, and temperature, respectively [1–4]. In contrast, there were few candidate materials, such as  $\text{Bi}_{1-x}\text{Sb}_x$  and  $\text{CsBi}_4\text{Te}_6$ , for low-temperature applications [5–7]. Thus, at low temperatures, a reduction in  $\kappa$  alone is not sufficient to achieve high thermoelectric performance, but an increase in  $S$  and a reduction in  $\rho$  are also essential.

Recently, one-dimensional van der Waals crystal  $\text{Ta}_4\text{SiTe}_4$  and its chemically substituted samples were reported to exhibit a significantly large  $|S|$  with sufficiently small  $\rho$  for thermoelectric materials over wide temperatures from 50 K

to room temperature [8].  $\text{Ta}_4\text{SiTe}_4$  has a strongly one-dimensional crystal structure consisting of  $\text{Ta}_4\text{SiTe}_4$  chains loosely bonded by van der Waals interactions between Te atoms, as shown in Fig. 1(a) [9,10]. This crystal structure has the orthorhombic  $Pbam$  symmetry, but is almost isotropic within the  $ab$  plane. The  $\text{Ta}_4\text{SiTe}_4$  chains are parallel to the  $c$  axis, forming an almost perfect triangular lattice in the  $ab$  plane, where the distances between neighboring chains differ by only 0.1%. Whisker crystals with a length of several millimeters and a maximum thickness of 10  $\mu\text{m}$  were synthesized by the crystal growth in the vapor phase, and  $\rho$  and  $S$  along the whisker,  $//c$ , were measured [8]. Furthermore, 0.1–0.2% Mo-doped whiskers exhibited a large negative Seebeck coefficient of  $|S| \sim 300$   $\mu\text{V K}^{-1}$  and a small  $\rho = 1$   $\text{m}\Omega \text{ cm}$  at 220–280 K, resulting in a huge power factor  $P = S^2/\rho$  of 170  $\mu\text{W cm}^{-1} \text{ K}^{-2}$ . This  $P$  is more than four times the room-temperature value for  $\text{Bi}_2\text{Te}_3$ -based practical materials.

Since the above report, research on this system as a thermoelectric material has increased. The whisker crystals of chemically doped  $\text{Nb}_4\text{SiTe}_4$ , which is a  $4d$  analog of  $\text{Ta}_4\text{SiTe}_4$ , and the solid solution between  $\text{Ta}_4\text{SiTe}_4$  and  $\text{Nb}_4\text{SiTe}_4$  also showed a large  $P$  exceeding those of practical materials [11,12]. Moreover,  $p$ -type whisker crystals were obtained by Ti doping at Ta sites [13]. The power factor of the  $p$ -type whiskers reached a maximum value of 60  $\mu\text{W cm}^{-1} \text{ K}^{-2}$  and exceeded the practical level between 100 K and room temperature. Furthermore, the thermoelectric properties of sintered  $\text{Ta}_4\text{SiTe}_4$  samples prepared by the cold-press method and a flexible composite of  $\text{Ta}_4\text{SiTe}_4$  whiskers and an organic conductor were investigated [14,15].

However, the physical background behind the realization of a huge  $P$  below room temperature in this system has not yet been clarified experimentally. First-principles calculations showed that  $\text{Ta}_4\text{SiTe}_4$  and  $\text{Nb}_4\text{SiTe}_4$  have a one-dimensional

\*yokamoto@issp.u-tokyo.ac.jp

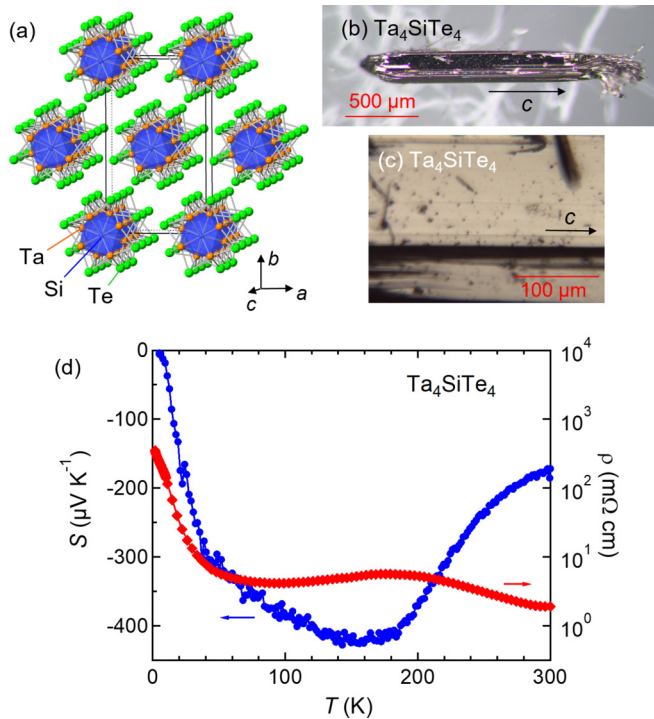


FIG. 1. (a) Crystal structure of  $\text{Ta}_4\text{SiTe}_4$ . The orthorhombic unit cell is indicated by solid lines. (b) A single crystal of  $\text{Ta}_4\text{SiTe}_4$ . (c) A typical crystal surface used in optical reflectivity measurements. (d) Seebeck coefficient and electrical resistivity of a  $\text{Ta}_4\text{SiTe}_4$  single crystal.

band structure, in which a small band gap opens at the Dirac point owing to strong spin-orbit coupling [8, 10, 16]. Naturally, this characteristic band structure plays an important role in achieving huge  $P$  at low temperatures. However, there have been few experimental studies on the electronic state and the correlation between the electronic state and thermoelectric properties of this system. Only the magnetoresistance measured along the chain direction and magnetic susceptibility of a nonoriented sample have been reported thus far [17–19]. The whisker morphology of the synthesized samples hampered the experimental studies. In this Letter, we report the reflectivity spectra of  $\text{Ta}_4\text{SiTe}_4$  single crystals measured over a wide energy range using linearly polarized light oscillating either parallel or perpendicular to the  $\text{Ta}_4\text{SiTe}_4$  chains, which enables us to obtain information on the one-dimensional electronic anisotropy. The optical conductivity  $\sigma(\omega)$  estimated from the reflectivity data showed two characteristic features that are closely related to the thermoelectric properties of  $\text{Ta}_4\text{SiTe}_4$ . One is a small energy gap of 0.1–0.15 eV-opening at the Fermi energy  $E_F$ . The other is an anisotropy in the low-energy region, where  $\sigma(\omega)$  parallel to the  $\text{Ta}_4\text{SiTe}_4$  chains is an order of magnitude higher than that perpendicular to them.

Single crystals of  $\text{Ta}_4\text{SiTe}_4$  were synthesized by crystal growth in the vapor phase. A mixture with a 2:1:2 molar ratio of Ta (Rare Metallic, 99.9%), Si (Kojundo Chemical Laboratory,  $\geq 99.9\%$ ), and Te (Rare Metallic, 99.999%) powders was sealed in an evacuated quartz tube with 10–20 mg of  $\text{TeCl}_4$  powder. The tube was heated to and kept at 873 K for 24 h and

1423 K for 96 h, and then furnace cooled to room temperature. We fabricated several hundred tubes to obtain single crystals for the reflectivity measurements, because the single crystals large enough were rarely obtained. Single crystals with a maximum width of 100  $\mu\text{m}$  or more and a length of several millimeters were used for the reflectivity measurements described below. A typical example is presented in Fig. 1(b). The obtained single crystals exhibited almost the same Seebeck coefficient and slightly higher electrical resistivity as those in the whisker crystals reported in a previous study [8], as shown in Fig. 1(d).

Normal incident reflectivity measurements were performed on the as-grown shiny surface at room temperature, using Fourier-type interferometers (0.02–0.06 eV, DA-8, ABB Bomen and 0.05–2.2 eV, FT/IR6600 IRT-5200) and a grating spectrometer (2–4 eV, MSV-5200) [20]. A typical surface used for the measurements is shown in Fig. 1(c). The reflectivity spectra were measured using linearly polarized light oscillating parallel or perpendicular to the  $\text{Ta}_4\text{SiTe}_4$  chains, that is, along the  $c$  axis. A  $\text{Ta}_4\text{SiTe}_4$  single crystal can easily bend and break under stress, reflecting the nature of the one-dimensional van der Waals crystals. This study used single crystals that were immediately after taken out from an evacuated quartz tube, which were confirmed to be free of cleavage and twisting. The crystal size was sufficient for optical measurements using microscopes designed for infrared and visible-ultraviolet spectrometers [20]. An evaporated Au or Ag film on a glass plate was used as a reference mirror. Reflectivity measurements in the visible- to visible-ultraviolet region were performed using synchrotron radiation at the BL3B beamline of the ultraviolet synchrotron orbital radiation facility (UVSOR), Institute for Molecular Science, Aichi, Japan. The spectrum was confirmed to be independent of its location within the spatial resolution. For quantitative discussion, the optical conductivity  $\sigma(\omega)$  was deduced from the reflectivity  $R(\omega)$  by the Kramers-Kronig transformation. This transformation requires appropriate extrapolation. An extrapolation below 0.02 eV was made according to the Hagen-Rubens equation and one above 30 eV assuming  $R \propto \omega^{-4}$ . Parameters in the Hagen-Rubens extrapolations  $\sigma(0)_{\text{HR}}$  were 180 and 38  $\Omega^{-1} \text{cm}^{-1}$  for the  $R(\omega)$  spectra taken parallel and perpendicular to the  $c$  axis, respectively.

First-principles density-functional calculations were performed on  $\text{Ta}_4\text{SiTe}_4$  using the QUANTUM ESPRESSO code [21, 22]. The calculations used norm-conserving pseudopotentials from the optimized norm-conserving Vanderbilt pseudopotential library [23] sourced from PSEUDODOJO [24]. The exchange-correlation function was treated within the generalized gradient approximation in the Perdew-Burke-Ernzerhof formalism [25]. The plane-wave energy cutoff for the wave functions was set to 92 Ry. Brillouin-zone integration was performed using a  $4 \times 2 \times 9k$ -point mesh. Electronic occupations were smeared with a Gaussian width of 0.002 Ry. In these calculations, the spin-orbit coupling was explicitly considered. The results of the density-functional calculations were used to calculate the optical conductivity spectra using the RESPACK code [26, 27]. In RESPACK, the optical conductivity is derived from a dielectric function based on a random-phase approximation. The energy cutoff of the dielectric function was set to 3 Ry. The integral over the

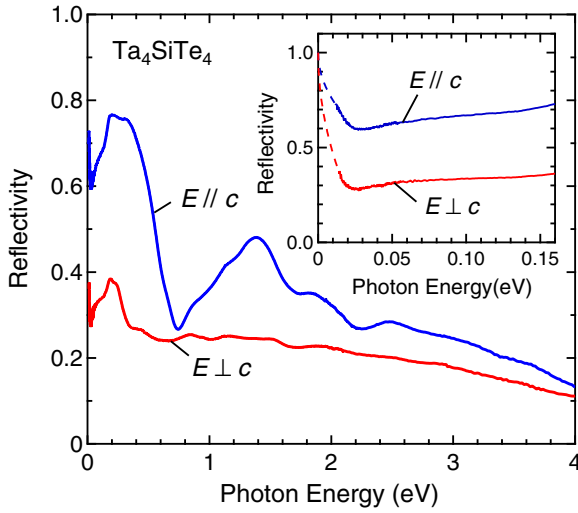


FIG. 2. Optical reflectivity spectra of a  $\text{Ta}_4\text{SiTe}_4$  single crystal for polarization parallel and perpendicular to the  $c$  axis measured at room temperature. The inset shows the enlarged spectra below 0.15 eV. The dotted lines are extrapolations using the Hagen-Rubens formula.

Brillouin zone was calculated using the generalized tetrahedron technique with a smearing of 0.01 eV.

Figure 2 shows the reflectivity spectra of a  $\text{Ta}_4\text{SiTe}_4$  single crystal measured at room temperature using linearly polarized light oscillating parallel to the  $c$  axis (the electric field  $E$  is parallel to the  $c$  axis, i.e.,  $E//c$ ) and perpendicularly to the  $c$  axis ( $E\perp c$ ). The reflectivity for  $E//c$ ,  $R_{//}(\omega)$ , shows a peak at approximately 1.4 eV and a strong increase below 0.7 eV. The latter increase most likely corresponds to the plasma edge of the metals. However,  $R_{//}(\omega)$  is considerably suppressed and decreased below 0.3 and 0.17 eV, respectively, in the midinfrared region, followed by a sharp increase below 0.03 eV. This complex spectral shape below the edge at 0.4 eV suggests that  $\text{Ta}_4\text{SiTe}_4$  is not a simple metal with Fermi surfaces, but has a complex structure in its band structure near  $E_F$ , as will be discussed later. The  $E\perp c$  reflectivity,  $R_{\perp}(\omega)$ , also showed a decrease below 0.17 eV and a sharp increase below 0.03 eV, similarly to  $R_{//}(\omega)$ . However, the  $R_{\perp}(\omega)$  values are lower than  $R_{//}(\omega)$  in the whole energies, and the increase in  $R_{\perp}(\omega)$  below 0.4 eV is significantly weaker than that in  $R_{//}(\omega)$  below 0.7 eV, probably reflecting an anisotropy in electrical conduction.

The optical conductivity spectra of  $\text{Ta}_4\text{SiTe}_4$  at room temperature obtained by performing the Kramers-Kronig transformation of the extrapolated reflectivity spectra are shown in Fig. 3(a). The optical conductivity for  $E//c$ ,  $\sigma_{//}(\omega)$ , exhibits peaks at 2.5, 1.9, 1.3, and 0.2 eV. The first three peaks in the near-infrared to visible region most likely correspond to the interband transitions. The last peak at 0.2 eV corresponds to the band gap at  $E_F$ , which will be discussed in detail below. In contrast, the optical conductivity for  $E\perp c$ ,  $\sigma_{\perp}(\omega)$ , also has a small peak at approximately 0.2 eV, but does not show a clear peak owing to the interband transition. These behaviors are good agreement with the theoretical result shown in Fig. 3(b). The theoretical spectrum for  $E//c$  has four prominent peaks at 2.5, 2.0, 1.4, and 0.4 eV, which correspond to those observed in the experimental spectrum shown in Fig. 3(a).

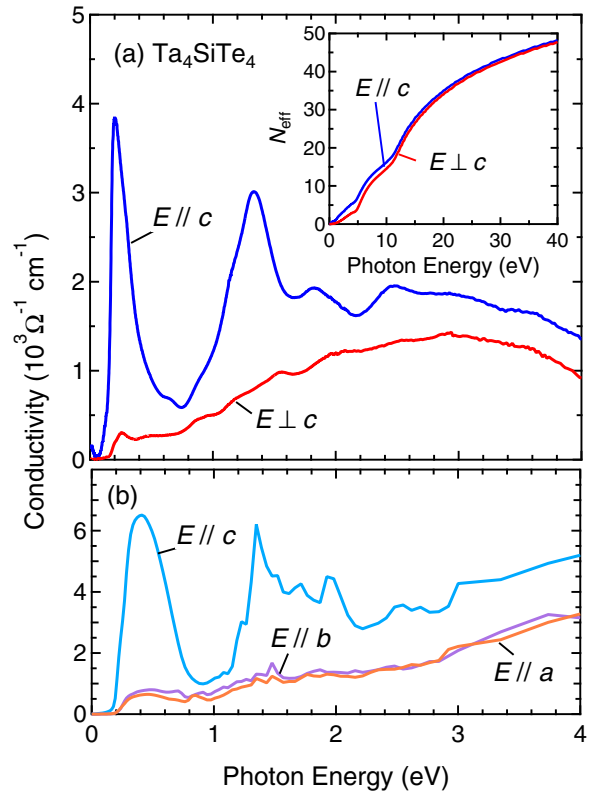


FIG. 3. (a) Optical conductivity spectra of a  $\text{Ta}_4\text{SiTe}_4$  single crystal parallel and perpendicular to the  $c$  axis at room temperature. The inset shows the effective number of electrons per formula unit. (b) Calculated optical conductivity spectra of  $\text{Ta}_4\text{SiTe}_4$  parallel to the  $a$ -,  $b$ -, and  $c$  axes.

The theoretical spectra of  $E//a$  and  $E//b$  are also consistent with the experimental  $\sigma_{\perp}(\omega)$ . The theoretical spectra of  $E//a$  and  $E//b$  are almost identical, which is natural considering the almost isotropic crystal structure within the  $ab$  plane, as discussed above, and have no significant structure other than a strong decrease below 0.2–0.4 eV. The experimental  $\sigma(\omega)$  of  $\text{Ta}_4\text{SiTe}_4$  also satisfies the summation rule. The inset of Fig. 3(a) shows the effective electron number per formula unit,  $N_{\text{eff}}$ , which is calculated as  $N_{\text{eff}} = \frac{2m_0V}{\pi e^2} \int_0^{\omega} \sigma(\omega') d\omega'$ , where  $m_0$  and  $V$  are the bare electron mass and the volume per formula unit, respectively. At sufficiently high energies,  $N_{\text{eff}}$  values for both  $E//c$  and  $E\perp c$  converge to 48, which is the number of valence electrons in the formula unit of  $\text{Ta}_4\text{SiTe}_4$ . These results indicate that the spectral analysis performed in this study, including extrapolation, is appropriate.

Subsequently, the low-energy  $\sigma(\omega)$  of  $\text{Ta}_4\text{SiTe}_4$ , which is closely related to its thermoelectric properties, is discussed. As shown in Fig. 4(a),  $\sigma_{//}(\omega)$  strongly increases from low values above 0.1 eV with increasing  $\omega$ . The  $\sigma_{\perp}(\omega)$  also increases above 0.15 eV, even though the change is weaker than that for  $E//c$ . The direct-independent increases of  $\sigma(\omega)$  above 0.1–0.15 eV indicate the presence of a small energy gap of 0.1–0.15 eV at  $E_F$ . The presence of such a small energy gap was implied by the Arrhenius plot of the electrical conductivity of the Ti-doped whiskers, where the carrier density was reduced by Ti doping [13]. A small band gap was also

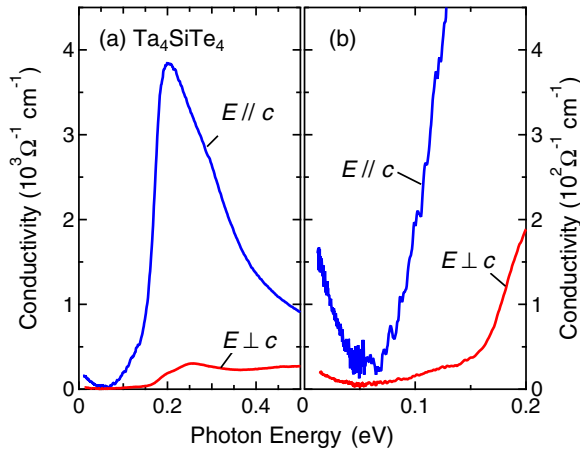


FIG. 4. Low-energy optical conductivity spectra of a  $\text{Ta}_4\text{SiTe}_4$  single crystal parallel and perpendicular to the  $c$  axis at room temperature. (a) and (b) show the optical conductivity spectra below 0.5 and 0.2 eV, respectively.

noted in first-principles calculations [8,16]. First-principles calculations without spin-orbit coupling showed that  $\text{Ta}_4\text{SiTe}_4$  is a Dirac semimetal with band-crossing points at  $E_F$ . When spin-orbit coupling is switched on, a small band gap of  $\sim 0.1$  eV opens at  $E_F$ . The strong increase in  $\sigma(\omega)$  above 0.1–0.15 eV is a direct observation of a spin-orbit gap opening at  $E_F$  in  $\text{Ta}_4\text{SiTe}_4$ .

In the topological semimetals with Dirac-like band dispersion in the vicinity of the  $E_F$ , a flat region often appears in the wide midinfrared energy region of the optical conductivity spectra [28,29]. They also show a Drude peak with a significantly narrow energy width owing to the presence of extremely light carriers. In contrast, a flat region does not exist in the optical conductivity spectra of  $\text{Ta}_4\text{SiTe}_4$ , probably because such a flat region is masked by the spin-orbit gap of 0.1–0.15-eV opening at  $E_F$ . The narrow Drude peak may correspond to a sharp increase in the optical conductivity in the lowest-energy region, which will be discussed later, but even lower-energy and lower-temperature measurements are needed to confirm it.

The existence of a small energy gap at  $E_F$  is closely related to the high thermoelectric performance at low temperatures of  $\text{Ta}_4\text{SiTe}_4$ . According to the  $10k_B T_{\text{max}}$  rule for thermoelectric materials, a relationship  $\Delta \sim 10k_B T_{\text{max}}$  exists between the size of the band gap  $\Delta$  and the optimum temperature for a thermoelectric material  $T_{\text{max}}$  in semiconductor thermoelectric materials [30]. In fact,  $\text{Bi}_2\text{Te}_3$ ,  $\text{PbTe}$ , and  $\text{SiGe}$ , with band gaps of 0.3, 0.5, and 0.7 eV have  $T_{\text{max}}$  of approximately 300, 500–700, and 1000 K, respectively [21]. The observed  $\Delta \sim 0.1$  eV in  $\text{Ta}_4\text{SiTe}_4$  suggests high thermoelectric performance at approximately 100 K in this material. However, it is difficult for a material to have such a significantly small  $\Delta$  at  $E_F$ , which is one of the reasons why thermoelectric conversion has not been utilized at low temperatures. For example,  $\text{CsBi}_4\text{Te}_6$ , which exhibits optimum performance at approximately 200 K, has a small  $\Delta$  due to the sparse existence of Bi–Bi bonds in its crystal structure [31]. In  $\text{Ta}_4\text{SiTe}_4$ , a spin-orbit gap opening at the Dirac point results in a small  $\Delta$ . The realization of a significantly small band gap can serve as a guideline for

finding a promising material for low-temperature applications that is yet to be utilized. This discussion indicates that the spin-orbit gap is a promising approach.

Below 0.05 eV,  $\sigma(\omega)$  of  $\text{Ta}_4\text{SiTe}_4$  for both  $E//c$  and  $E\perp c$  gradually increases toward the lowest energy, as shown in Fig. 4(b), which is probably the Drude peak associated with the itinerant electrons. As a result,  $\sigma_{//}(\omega)$  at the lowest energy of 0.02 eV is equal to  $160 \Omega^{-1} \text{cm}^{-1}$ , which is approximately one-sixth of the dc electrical conductivity of  $1000 \Omega^{-1} \text{cm}^{-1}$  measured using a whisker crystal [8]. Although the origin of this discrepancy is not fully understood,  $\sigma(\omega)$  may continue to increase below 0.02 eV toward  $\hbar\omega = 0$ , resulting in a smaller discrepancy between  $\sigma(0)$  and the dc conductivity. In this case, the increase in  $\sigma(\omega)$  toward  $\hbar\omega = 0$  indicates the presence of a small amount of strongly light-conducting carriers.

Although the quantitative estimate of the lowest-energy  $\sigma(\omega)$  remains ambiguous, as discussed above,  $\sigma_{\perp}(\omega) = 20 \Omega^{-1} \text{cm}^{-1}$  at  $\hbar\omega = 0.02$  eV is one-eighth of  $\sigma_{//}(\omega)$ , as shown in Fig. 4(b), suggesting the presence of an anisotropy of one order of magnitude in the electrical conduction of  $\text{Ta}_4\text{SiTe}_4$ . Although this anisotropy appears weak, considering that  $\text{Ta}_4\text{SiTe}_4$  is a one-dimensional van der Waals crystal, this result demonstrates the presence of anisotropic electron conduction in  $\text{Ta}_4\text{SiTe}_4$ .

The observed weak one-dimensional anisotropy, i.e., one order of magnitude higher  $\sigma_{//}$  than  $\sigma_{\perp}$ , may play an important role in realizing high thermoelectric performance in  $\text{Ta}_4\text{SiTe}_4$ . Hicks and Dresselhaus theoretically indicated that systems with one-dimensional electron conduction can exhibit considerably higher thermoelectric performance than three-dimensional systems by considering the confinement of electrons in nanosized quantum wires [32]. This effect is expected to work similarly for bulk materials with one-dimensional anisotropy of electron conduction, as discussed for  $\text{CsBi}_4\text{Te}_6$  [6,7,31]. However, one-dimensional electron conduction is weak against disorder. External factors such as lattice defects have a significant negative effect on one-dimensional electron conduction due to Anderson localization. In contrast, electron conduction in  $\text{Ta}_4\text{SiTe}_4$  is robust against disorder. For example, the whisker samples of  $\text{Ta}_4\text{SiTe}_4\text{-Nb}_4\text{SiTe}_4$  solid solution show similar or smaller  $\rho$  than that of the end members [12]. The moderate one-dimensional anisotropy in  $\text{Ta}_4\text{SiTe}_4$  plays an important role in realizing the robustness of electron conduction in  $\text{Ta}_4\text{SiTe}_4$ , which results in high thermoelectric performance in this system. Recently, materials with one-dimensional crystal structure were found to exhibit high thermoelectric performance below room temperature [33–36], implying the importance of anisotropic electrical conduction.

In conclusion, we measured the reflectivity of synthesized single crystals of a one-dimensional van der Waals crystal  $\text{Ta}_4\text{SiTe}_4$  that show high thermoelectric performance at low temperatures over a wide energy range. The optical conductivity data estimated from the reflectivity spectra indicated the presence of a small band gap of 0.1–0.15 eV at  $E_F$ , corresponding to the spin-orbit gap predicted in the first-principles calculations. At the lowest measured energy,  $\sigma_{//}(\omega)$  is one order of magnitude higher than  $\sigma_{\perp}(\omega)$ , indicating the presence of moderate anisotropy in the electrical conduction of  $\text{Ta}_4\text{SiTe}_4$ .

This significantly small band gap and the weak but robust one-dimensional anisotropy in electrical conduction play key roles in the high thermoelectric performance, particularly the observed gigantic power factor in  $\text{Ta}_4\text{SiTe}_4$  below room temperature. The coexistence of these two factors in a material is a promising strategy for developing practical materials for low-temperature applications.

We are grateful to Y. Yoshikawa and Y. Abe for their help with single-crystal growth and K. Nakamura for his

help with the first-principles calculations. Part of this work was performed at the BL3B of the UVSOR Synchrotron Facility, Institute for Molecular Science (IMS program 21–637). This work was partly supported by JSPS KAKENHI (Grants No. 19H05823, No. 20H00346, No. 20H02603, No. 22H04953, No. 23H01831, and No. 23H04871), JST ASPIRE (Grant No. JPMJAP2314), and the Research Foundation for the Electrotechnology of Chubu. Part of the computation was performed at the Supercomputer Center, Institute for Solid State Physics, the University of Tokyo, Japan.

- 
- [1] K. Biswas, J. He, I. D. Blum, C.-I. Wu, T. P. Hogan, D. N. Seidman, V. P. Dravide, and M. G. Kanatzidis, *Nature (London)* **489**, 414 (2012).
- [2] K. F. Hsu, S. Loo, F. Guo, W. Chen, J. S. Dyck, C. Uher, T. Hogan, E. K. Polychroniadis, and M. G. Kanatzidis, *Science* **303**, 818 (2004).
- [3] L.-D. Zhao, S.-H. Lo, Y. Zhang, H. Sun, G. Tan, C. Uher, C. Wolverton, V. P. Dravid, and M. G. Kanatzidis, *Nature (London)* **508**, 373 (2014).
- [4] C. Chang, M. Wu, D. He, Y. Pei, C.-F. Wu, X. Wu, H. Yu, F. Zhu, K. Wang, Y. Chen, L. Huang, J.-F. Li, J. He, and L.-D. Zhao, *Science* **360**, 778 (2018).
- [5] W. M. Yim and A. Amith, *Solid State Electron.* **15**, 1141 (1972).
- [6] D.-Y. Chung, T. Hogan, P. Brazis, M. Rocci-Lane, C. Kannewurf, M. Bastea, C. Uher, and M. G. Kanatzidis, *Science* **287**, 1024 (2000).
- [7] D.-Y. Chung, T. P. Hogan, M. Rocci-Lane, P. Brazis, J. R. Ireland, C. R. Kannewurf, M. Bastea, C. Uher, and M. G. Kanatzidis, *J. Am. Chem. Soc.* **126**, 6414 (2004).
- [8] T. Inohara, Y. Okamoto, Y. Yamakawa, A. Yamakage, and K. Takenaka, *Appl. Phys. Lett.* **110**, 183901 (2017).
- [9] M. E. Badding and F. J. DiSalvo, *Inorg. Chem.* **29**, 3952 (1990).
- [10] J. Li, R. Hoffmann, M. E. Badding, and F. J. DiSalvo, *Inorg. Chem.* **29**, 3943 (1990).
- [11] Y. Okamoto, T. Wada, Y. Yamakawa, T. Inohara, and K. Takenaka, *Appl. Phys. Lett.* **112**, 173905 (2018).
- [12] Y. Yoshikawa, T. Wada, Y. Okamoto, Y. Abe, and K. Takenaka, *Appl. Phys. Express* **13**, 125505 (2020).
- [13] Y. Okamoto, Y. Yoshikawa, T. Wada, and K. Takenaka, *Appl. Phys. Lett.* **115**, 043901 (2019).
- [14] Q. Xu, S. Qu, C. Ming, P. Qiu, Q. Yao, C. Zhu, T.-R. Wei, J. He, X. Shi, and L. Chen, *Energy Environ. Sci.* **13**, 511 (2020).
- [15] Q. Xu, C. Ming, T. Xing, P. Qiu, J. Xiao, X. Shi, and L. Chen, *Mater. Today Phys.* **19**, 100417 (2021).
- [16] S. Liu, H. Yin, D. J. Singh, and P.-F. Liu, *Phys. Rev. B* **105**, 195419 (2022).
- [17] M. E. Badding, R. L. Gitzendanner, R. P. Ziebarth, and F. J. DiSalvo, *Mater. Res. Bull.* **29**, 327 (1994).
- [18] A. Stolovits, A. Sherman, K. Ahn, and R. K. Kremer, *Phys. Rev. B* **62**, 10565 (2000).
- [19] A. Stolovits, K. Ahn, R. K. Kremer, and A. Sherman, *Synth. Met.* **121**, 1267 (2001).
- [20] K. Takenaka, M. Tamura, N. Tajima, H. Takagi, J. Nohara, and S. Sugai, *Phys. Rev. Lett.* **95**, 227801 (2005).
- [21] P. Giannozzi, S. Baroni, N. Bonini, M. Calandra, R. Car, C. Cavazzoni, D. Ceresoli, G. L. Chiarotti, M. Cococcioni, I. Dabo, A. D. Corso, S. de Gironcoli, S. Fabris, G. Fratesi, R. Gebauer, U. Gerstmann, C. Gougoussis, A. Kokalj, M. Lazzeri, L. Martin-Samos, N. Marzari, F. Mauri, R. Mazzarello, S. Paolini, A. Pasquarello, L. Paulatto, C. Sbraccia, S. Scandolo, G. Sclauzero, A. P. Seitsonen, A. Smogunov, P. Umeri, and R. M. Wentzcovitch, *J. Phys.: Condens. Matter* **21**, 395502 (2009).
- [22] P. Giannozzi, O. Andreussi, T. Brumme, O. Bunau, M. B. Nardelli, M. Calandra, R. Car, C. Cavazzoni, D. Ceresoli, M. Cococcioni, N. Colonna, I. Carnimeo, A. Dal Corso, S. de Gironcoli, P. Delugas, R. A. DiStasio, Jr., A. Ferretti, A. Floris, G. Fratesi, G. Fugallo, R. Gebauer, U. Gerstmann, F. Giustino, T. Gorni, J. Jia, M. Kawamura, H.-Y. Ko, A. Kokalj, E. Küçükbenli, M. Lazzeri, M. Marsili, N. Marzari, F. Mauri, N. L. Nguyen, H.-V. Nguyen, A. Otero-de-la-Roza, L. Paulatto, S. Poncé, D. Rocca, R. Sabatini, B. Santra, M. Schlipf, A. P. Seitsonen, A. Smogunov, I. Timrov, T. Thonhauser, P. Umari, N. Vast, X. Wu, and S. Baroni, *J. Phys.: Condens. Matter* **29**, 465901 (2017).
- [23] D. R. Hamann, *Phys. Rev. B* **88**, 085117 (2013) [**95**, 239906(E) (2017)].
- [24] M. J. van Setten, M. Giantomassi, E. Bousquet, M. J. Verstraete, D. R. Hamann, X. Gonze, and G.-M. Rignanese, *Comput. Phys. Commun.* **226**, 39 (2018).
- [25] J. P. Perdew, K. Burke, and M. Ernzerhof, *Phys. Rev. Lett.* **77**, 3865 (1996).
- [26] K. Nakamura, Y. Yoshimoto, Y. Nomura, T. Tadano, M. Kawamura, T. Kosugi, K. Yoshimi, T. Misawa, and Y. Motoyama, *Comput. Phys. Commun.* **261**, 107781 (2021).
- [27] K. Nakamura, Y. Yoshimoto, Y. Nohara, and M. Imada, *J. Phys. Soc. Jpn.* **79**, 123708 (2010).
- [28] M. B. Schilling, L. M. Schoop, B. V. Lotsch, M. Dressel, and A. V. Pronin, *Phys. Rev. Lett.* **119**, 187401 (2017).
- [29] Z. Qiu, C. Le, Z. Liao, B. Xu, R. Yang, J. Hu, Y. Dai, and X. Qiu, *Phys. Rev. B* **100**, 125136 (2019).
- [30] G. D. Mahan, *Solid State Physics* (Academic Press, New York, 1997), Vol. 51, pp. 81–157.
- [31] P. Larson, S. D. Mahanti, D.-Y. Chung, and M. G. Kanatzidis, *Phys. Rev. B* **65**, 045205 (2002).
- [32] L. D. Hicks and M. S. Dresselhaus, *Phys. Rev. B* **47**, 16631(R) (1993).
- [33] A. Nakano, Y. Maruoka, F. Kato, H. Taniguchi, and I. Terasaki, *J. Phys. Soc. Jpn.* **90**, 033702 (2021).
- [34] A. Nakano, A. Yamakage, U. Maruoka, H. Taniguchi, Y. Yasui, and I. Terasaki, *J. Phys. Energy* **3**, 044004 (2021).

- [35] Q.-x. Dong, Y.-f. Huang, L.-b. Zhang, J.-l. Bai, J.-w. Cheng, Q.-y. Liu, P.-y. Liu, C.-d. Li, J.-s. Xiang, J.-f. Wang, B.-B. Ruan, Z.-a. Ren, P.-j. Sun, and G.-f. Chen, [Appl. Phys. Lett.](#) **122**, 094104 (2023).
- [36] Q. Dong, J. Xiang, Z. Wang, Y. Li, R. Lu, T. Zhang, N. Chen, Y. Huang, Y. Wang, W. Zhu, G. Li, H. Zhao, X. Zheng, S. Zhang, Z. Ren, J. Yang, G. Chen, and P. Sun, [Sci. Bull.](#) **68**, 920 (2023).